International Journal on Magnetic Particle Imaging
Vol 12, No 1, Suppl 1, Article ID 2603046, 3 Pages

Infinite Science Publishing

Proceedings Article

Development of a Compact FFL-MPI System Based on a Halbach Permanent Magnet

Z. Hou[a,b] · F. Lia[a,b] · Y. Wang[a,b] · Y. Xu[a,b] · H. Lv[a] · L. Dong[a] · Y. Yang[a,b] · W. Feng[a,b] · J. Guo[a,b] · Z. Wu[a,b,*] · J. Zheng[a,b]

[a]Shandong Laboratory of Advanced Biomaterials and Medical Devices in Weihai, Weihai 264210, China
[b]Suzhou Institute of Biomedical Engineering and Technology, Chinese Academy of Sciences, Suzhou 215163, China
*Corresponding author, email: wuzy@sibet.ac.cn

Abstract

The high power consumption and large size of conventional Magnetic Particle Imaging (MPI) systems present significant barriers to their clinical translation. To address this challenge, we present a novel, compact MPI scanner implementation based on a Halbach permanent magnet structure. This design generates a field-free line (FFL) and achieves a gradient strength of 1.16 T/m within a 50 mm diameter bore. Experimental results demonstrate that the system successfully resolves two distinct particle points separated by 1 mm, confirming a spatial resolution better than 1 mm. Our findings position this low-power, Halbach-based MPI scanner as a promising tool for molecular imaging laboratories and a significant step towards future human-scale applications.

I. Introduction

The high power consumption of high-gradient MPI systems, which necessitates substantial space, energy, and additional water cooling equipment, represents a major obstacle to scaling MPI for human applications[1-4]. To overcome the power limitations of MPI, this study proposes a novel scanner implementation based on a Halbach magnet structure. By leveraging the efficient magnetic field generation characteristics of this structure, the system achieves reduced energy consumption and a more compact form factor, paving the way for broader adoption in human experiments. This design achieves a spatial resolution of 1 mm in small field-of-view (FOV) imaging, positioning it as a valuable addition to molecular laboratories and highlighting the promising potential of MPI in the field of molecular imaging.

II. Methods and materials

As shown in Figure 1, the system is capable of accommodating samples up to 50 mm in diameter. A rotating gantry supports the permanent magnet assembly responsible for gradient field generation, with the excitation and detection coil assembly fixed inside. All components are integrated onto a non-magnetic optical platform.

The magnet assembly features a two-layer Halbach ring configuration, with each layer comprising 16 NdFeB permanent magnets. Each magnet measures 23×23 ×50 mm, with a remanence *Br* of 1.33 T and a coercivity *Hcj* of 12 kOe, as illustrated in Figure 2. The magnets are mounted using non-magnetic fixtures and interconnected via non-magnetic bearings.

Through comprehensive optimization considering system dimensions, target FOV, and magnetic performance requirements, the final magnet's inner diameter, outer diameter, and height were determined to be 78 mm,

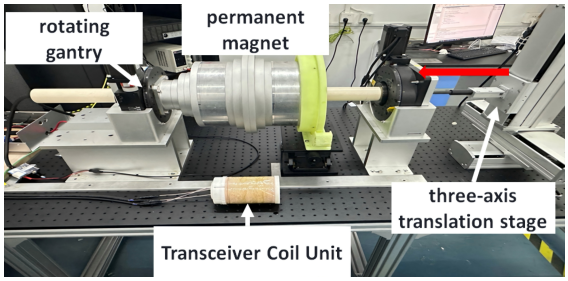

Figure 1: Realized FFL scanner.The magnet is positioned at the center of the system, with the transmit and receive coils located inside it. The magnet is mounted between two rotating gantries, and a rotary motor drives its rotation to achieve FFL sweeping. The sample stage is a three-axis motorized translation stage, with the sample loading direction indicated by the red arrow in the figure.

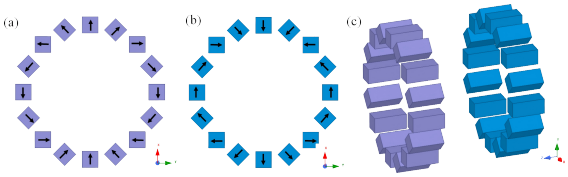

Figure 2: Exploded view of the two-layer Halbach cylinder magnet assembly. (a) and (b) show the magnetization directions of two layers of Halbach magnets, respectively, where the black arrows indicate the magnetization direction. (c) depicts the spatial arrangement of these two layers of Halbach magnets.

112 mm, and 50 mm, respectively. The spacing between the two Halbach rings is 107 mm. The magnetic field gradient measured in the 50 mm diameter central region using a Gaussmeter (CH3600, Beijing Cuihai) is 1.16 T/m. The corresponding magnetic field distribution is shown in Figure 3.

In the initial experiments, imaging was only performed over a 9 mm×9mm field of view, so no additional selection field coil was required. Both the excitation and receiver coils were constructed as solenoids and housed within a plastic sleeve. The excitation coil operated at 5.95 kHz with a 14 mT amplitude, thereby sufficiently covering the entire imaging area. Its impedance was matched using high-voltage ceramic capacitors. During operation, the coil drew a peak current of 7 A; its equivalent circuit consisted of a 0.85 Ω resistor in series with a 1.0 mH inductor. After series matching with a 0.73 μF capacitor, the total impedance magnitude was reduced to 1.1Ω. The resulting active power consumption was 20.8 W, with an apparent power of 26.95 VA.

To suppress signal feedthrough, the receiver coil adopts a first-order gradiometer configuration incorporating a counter-wound compensation coil of identical dimensions. This setup provides preliminary cancellation of the fundamental excitation signal. The signal was

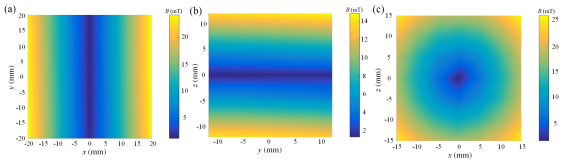

Figure 3: Magnetic field of the optimized Halbach magnet from Figure 2. (a), (b), and (c) show the magnetic field distributions in the x-y plane, y-z plane, and x-z plane, respectively.

then passed through a 10 kHz high-pass filter (EF121, Thorlabs) to remove residual feedthrough, before being directed to a low noise amplifier (SR560, Stanford Research Systems). The SR560 amplified the particle signal by a factor of 100 and applied its integrated 12th-order 300 kHz low pass filter to suppress high-frequency noise. Finally, the conditioned analog signal was digitized by a data-acquisition card (USB-6363, National Instruments) and transferred to a host computer for subsequent processing and analysis.

By scanning the imaging range and measuring the signals of delta particles, calibration data are obtained. Before combining the calibration data into the system matrix, preprocessing is required. First, multiple repeated measurements of the signals are averaged to improve the signal-to-noise ratio. Then, data trimming (removal of unstable segments), background signal correction and Fourier transform are performed sequentially.

Each calibration data has a size of $[N_\theta, N_k]$, representing the number of angles and frequency points, respectively. Finally, the data from 20 calibration points acquired over a 180° angular range via mechanical rotation are combined to form the system matrix of size $N_\theta \times N_k \times N_r$. The acquisition time was set to 10 s per point, resulting in a total duration of 200 s. After obtaining the system matrix and the measured signal, we employed an improved Kaczmarz algorithm for image reconstruction. Addressing the severe ill-posedness of the MPI system matrix and the significant energy disparity between frequency components, this method integrates row-norm weighted preconditioning with a hybrid regularization mechanism.

We modeled the reconstruction process as a constrained optimization problem within the complex domain. To balance the gradient contributions of high and low-frequency signals and recover fine spatial details, a weighted least-squares data fidelity term was constructed. Additionally, L_1 and L_2 norms were jointly introduced to induce sparsity and smoothness in the solution, thereby effectively suppressing measurement noise. Unlike traditional algebraic reconstruction techniques that rely on fixed relaxation parameters, this approach utilizes the Adam optimizer. By leveraging the first and second moments of the gradients, the algorithm adaptively adjusts the step size for each voxel, accelerating

10.18416/ijmpi.2026.2603046

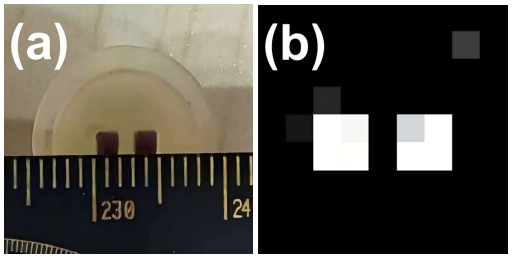

Figure 4: Experimental validation of sub-millimeter spatial resolution. (a) The fabricated resolution phantom. (b) The corresponding reconstruction, showing two distinctly resolved particle points with 1 mm separation, achieved within a 9 mm × 9 mm field of view.

convergence and minimizing oscillation.The reconstruction objective function is formulated as follows:

$$\hat{\mathrm{x}} = \underset{\mathrm{x}\in\mathbb{R}^N, \mathrm{x}\geq 0}{arg\,min} \left(\frac{1}{M} \|\mathrm{W}(\mathrm{Ax}-\mathrm{b})\|_2^2 + \lambda_{reg}\|\mathrm{x}\|_2^2 + \lambda_{l1}\|\mathrm{x}\|_1 \right),$$

where $\mathrm{W} = diag(w_1, w_2, \ldots, w_M)$ represents the row-weighting matrix. The diagonal elements w_i are determined by the inverse potential of the system matrix row norms to compensate for weak high-frequency responses:

$$w_i = \left(\frac{\|\mathrm{A}_i\|_2}{\max_k \|\mathrm{A}_k\|_2} \right)^{-\gamma},$$

where, $\mathrm{A} \in \mathbb{C}^{M\times N}$ denotes the system matrix, with A_i representing its i-th row vector, while $\mathrm{b} \in \mathbb{C}^M$ corresponds to the measured frequency-domain voltage signals. The vector $\mathrm{x} \in \mathbb{R}^N$ signifies the spatial distribution of magnetic nanoparticle concentration to be reconstructed. Furthermore, λ_{reg} and λ_{l1} serve as the coefficients for L_2 (Ridge) and L_1 sparse regularization, respectively, and γ acts as the weighting exponent factor designed to tune the amplification of weak signal components.

III. Results and discussion

Figure 4(a) shows the fabricated resolution phantom consisting of two cubic samples (side length: 2 mm) filled with synomag70 particles at an iron concentration of 10 mg/mL. This corresponds to an iron content of 0.08 mg per sample (0.16 mg total). Figure 4(b) presents the reconstructed image acquired over 239 s, demonstrating the system's capability to clearly resolve the two samples separated by 1 mm. These results indicate that the system achieves a spatial resolution better than 1 mm. The experiment successfully realized an imaging field of view measuring 9 mm × 9 mm.

The long-term stability of the permanent magnet subsystem is ensured through both environmental control and deliberate design. All experiments were conducted in a climate-controlled laboratory to minimize the effect of temperature fluctuations on the NdFeB magnets. Regarding the risk of demagnetization, it is effectively mitigated by the adopted sparse Halbach configuration of the selection field magnet and the sufficient physical separation between the excitation coil and the magnet arrays, which keeps the alternating field strength at the magnets well below their coercivity.

IV. Conclusion

This study details the successful development of a Halbach-based FFL-MPI system prototype. The system achieved high-resolution imaging of phantoms at 1 mm spatial resolution while operating under a 1.16 T/m gradient strength with a remarkably low power consumption of 20.8 W. Subsequent work will focus on three key enhancements to advance system performance and stability. First, a pair of Maxwell coils will be integrated to generate a spatially uniform drive field, enabling electronic translation of the FFL and expanding the scannable field of view to the full 50 mm diameter of the bore. Second, a dedicated temperature-control system will be implemented to minimize thermal drift of the magnetic field. Finally, a periodic magnetic-field monitoring and calibration routine will be established to safeguard against long-term performance degradation (e.g., from magnet aging or demagnetization). This will ensure sustained imaging accuracy over extended operation.

Acknowledgments

This work was supported in part by the Department of Science and Technology of Shandong Province under grant No.SYS202208 and the SIBET Innovation Priority Project under grant E4550305.

Author's statement

Conflict of interest: Authors state no conflict of interest.

References

[1] Weber M , et al.*Novel Field Geometry Using Two Halbach Cylinders for FFL-MPI.* International Journal on Magnetic Particle ImagingVol. 4 No. 2 2018.DOI:10.18416/IJMPI.2018.1811004.

[2] Franke, J. et al. *System Characterization of a Highly Integrated Preclinical Hybrid MPI-MRI Scanner.* IEEE Transactions on Medical Imaging 35, 1993–2004. doi:10 . 1109 / tmi . 2016 . 2542041 (2016).

[3] Knopp, T., & Buzug, T. M. *Magnetic Particle Imaging: An Introduction to Imaging Principles and Scanner Instrumentation.* 2012.

[4] Mattingly, Eli, et al. *Design, construction and validation of a magnetic particle imaging (MPI) system for human brain imaging.* Physics in Medicine & Biology 70.1 (2025): 015019. DOI: 10.1088/1361-6560/ad9db0

